DOI:
10.1021/acs.biochem.0c00502

An unusually rapid protein backbone modification stabilizes the essential bacterial enzyme MurA

Tianze Zhang, Kjetil Hansen, Argyris Politis, Manuel M. Müller*

Address: Department of Chemistry, King's College London 7 Trinity Street, London, SE1 1DB (UK)

**Correspondence to M.M.M. (manuel.muller@kcl.ac.uk)*

ABSTRACT: Proteins are subject to spontaneous rearrangements of their backbones. Most prominently, asparagine and aspartate residues isomerize to their β-linked isomer, isoaspartate (isoAsp), on time scales ranging from days to centuries. Such modifications are typically considered "molecular wear-and-tear", destroying protein function. However, the observation that some proteins, including the essential bacterial enzyme MurA, harbor stoichiometric amounts of isoAsp suggests that this modification can confer advantageous properties. Here we demonstrate that nature exploits an isoAsp residue within a hairpin to stabilize MurA. We found that isoAsp formation in MurA is unusually rapid and critically dependent on folding status. Moreover, perturbation of the isoAsp-containing hairpin via site-directed mutagenesis causes aggregation of MurA variants. Structural mass spectrometry revealed that this effect is caused by local protein unfolding in MurA mutants. Our findings demonstrate that MurA evolved to "mature" via a spontaneous post-translational incorporation of a β-amino acid, which raises the possibility that isoAsp-containing hairpins may serve as a structural motif of biological importance.

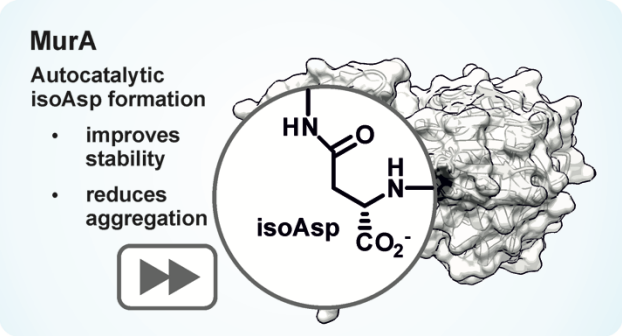

(For Table of Contents use only)

INTRODUCTION

Proteins are usually assembled from 20 different α-amino acids, linked via amide bonds in a sequence-specific manner. The polyamide backbone is often considered invariant and inert. Nevertheless, over typical protein lifetimes, asparagine (Asn) and aspartate (Asp) residues can spontaneously isomerize into isoAspartate (isoAsp) featuring an unusual β-peptidic linkage (**Figure 1a**)[1-3]. This process is initiated by the nucleophilic attack of the (deprotonated) backbone amide nitrogen on the side chain amide or acid group in the case of Asn and Asp, respectively. The resulting succinimide intermediate hydrolyses with a slight preference (70-85%) in the alpha position, yielding a mixture of isoAsp and Asp residues[1]. In model peptides, this process occurs on timescales ranging from days to years, with Asn-Gly sequences rearranging most rapidly[4]. The rates are typically lower in proteins, especially for Asn residues that are embedded in secondary structure motifs or otherwise engaged in H-bonds involving the N-H of the i+1 residue[5].

IsoAsp formation is considered as protein damage and associated with several pathologies[6]. For example, isoAsp is thought to promote aggregation of Aβ in neurodegenerative diseases[7-9] and of eye lens crystallins[10] in cataract formation. To counteract the negative effects of isoAsp formation, nature has evolved a 'repair' enzyme, protein *L*-isoaspartyl methyltransferase (PIMT)[11, 12]. PIMT-dependent methylation at the α-carboxylate promotes succinimide formation and subsequent hydrolysis into a mixture of Asp and isoAsp (**Figure 1a**). Successive repair cycles are thus required to fully convert isoAsp to Asp. The importance of PIMT is demonstrated by the observation that PIMT-knockout mice, which accumulate isoAsp in their proteome, exhibit many adverse phenotypes such as retarded growth, reduced lifespan, and seizures[13, 14].

Remarkably, the essential bacterial enzyme MurA has been shown to contain an isoAsp residue within a hairpin (**Figure 1b**)[3], although it is unknown whether this β-linked residue plays a functional role. MurA, a UDP-N-acetylglucosamine 1-carboxyvinyltransferase, is a cytosolic enzyme and antibiotic target that catalyzes the first committing step in cell wall biosynthesis[15]. Careful structural analysis by Eschenburg and Schönbrunn using X-ray crystallography has revealed that MurA from *Enterobacter cloacae* exhibits an isoAsp residue in an unusual beta hairpin[3]. IsoAsp67, which arises from deamidation/rearrangement of Asn67, perfectly fits the electron density at this site (**Figure 1b**), whereas Asn is not accommodated by the electron density (**Figure S1a**) and exhibits unfavorable dihedral angles (**Figure S1b,c**). The sequence of the hairpin encompassing isoAsp67 is present in

Enterobacteriaceae and *Vibrionaceae* (**Figure 1c**), where it forms an atom-efficient way to access this hairpin. In other structurally characterized MurA homologs more residues are needed to provide a similar structure.

β-peptidic linkages have been shown to provide unique structural features, primarily in the context of foldamers[16, 17]. Such observations raise the possibility that isoAsp can provide access to unusual structural motifs and therefore confer favorable properties onto proteins. Here we demonstrate that this is indeed the case for the naturally occurring isoAsp residue in MurA. We show that mutations precluding isoAsp formation at position 67 in MurA promote protein aggregation and negatively impact on MurA activity. Moreover, we found isoAsp in MurA increases protein stability by rigidifying the movement of neighboring regions. Therefore, the conversion of Asn67 to isoAsp represents a desirable protein backbone 'maturation' process, rather than molecular wear-and-tear which is commonly associated with isoAsp formation.

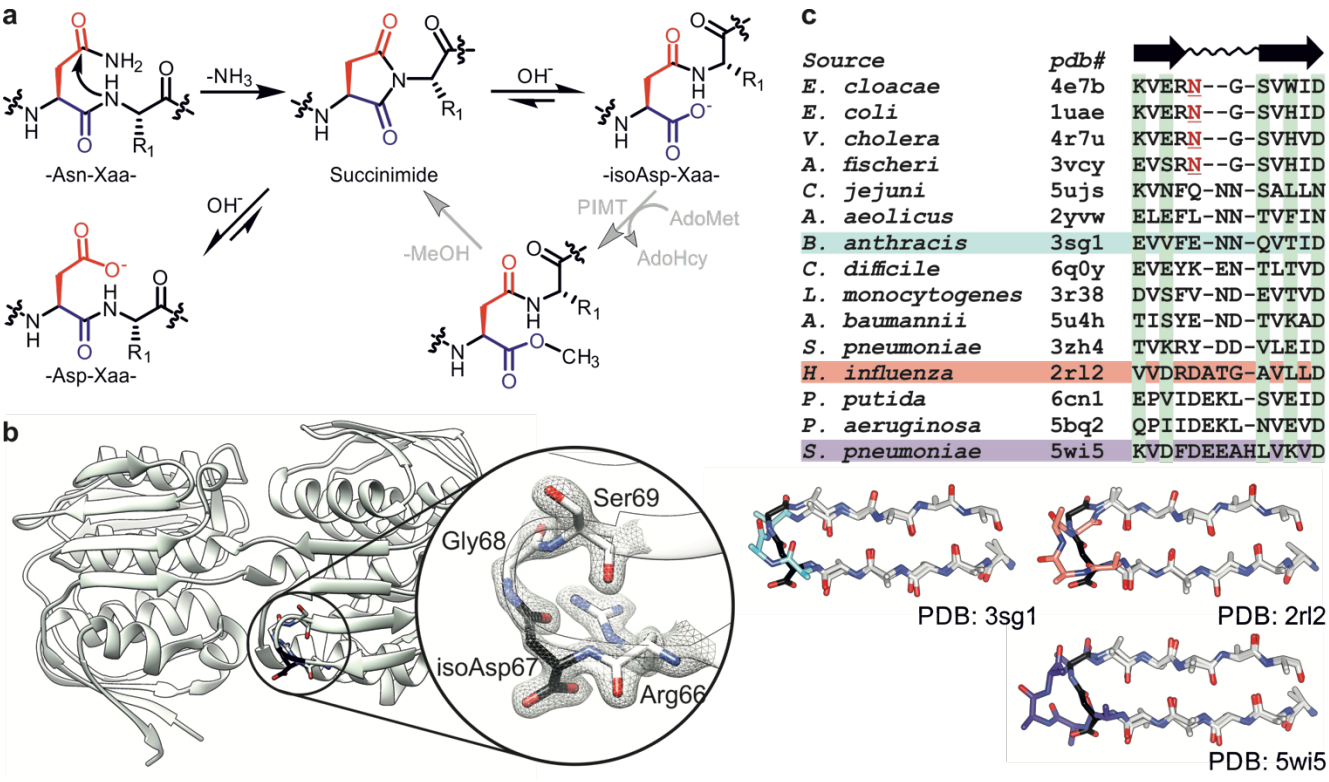

Figure 1: Formation of isoAspartate and occurrence in MurA. a *Mechanism of the spontaneous formation and enzyme-catalysed repair of isoaspartate (isoAsp). Deamidation of asparagine occurs by nucleophilic attack of the amino group of the C-flanking amino acid. This process leads to formation of a metastable succinimide intermediate, which hydrolyses to a mixture of Asp and isoAsp linkages. isoAsp can be methylated by PIMT to promote succinimide formation and in turn revert some*

proportions to Asp (grey arrows). AdoMet: S-adenosylmethionine; AdoHcy: S-adenosylhomocysteine. ***b*** *The essential bacterial enzyme MurA features an isoAsp residue (black) in a hairpin, formed post-translationally from Asn67 (pdb: 1ejc)[3].* ***c*** *Sequence alignment of structurally characterized MurA variants. Residues that align with the solvent-facing residues of the β-sheet from the E. cloacae variant are shown in green. The isoAsp-containing hairpin is conserved in Enterobacteriaceae and Vibrionaceae. Alternative hairpin sequences are possible, albeit with a requirement for additional residues. Example β-hairpins with one (B. anthracis, 3sg1, light blue[18]), two (H. influenza, 2rl2, salmon[19]), and three (S. pneumoniae, 5wi5, purple[20]) additional residues were superimposed with the structure from E. cloacae (4e7b, black) and are shown on the right. β-Sheet residues are shown in grey and side chains omitted for clarity.*

METHODS

Production and purification of MurA

Plasmids encoding MurA variants were transformed into BL21(DE3) for protein production. 600 mL LB containing 100 µg/mL of ampicillin were inoculated with overnight cultures and grown at 37 °C with shaking at 220 rpm. When an OD_{600} of 0.5-0.8 was reached, protein production was induced with 1 mM IPTG, and the cultures incubated for an additional 3.5-4 h at 37 °C with shaking. Cells were then pelleted by centrifugation (4,200 rpm, 20 min, 4 °C). The pellets were resuspended in lysis buffer (50 mM Tris-HCl, 200 mM NaCl, pH 7.6) at room temperature, transferred to 50 mL conical tubes and centrifuged again at 2211 rcf. The resulting cell pellets were stored at -20 °C.

Harvested cell pellets were resuspended in 20 mL of chilled lysis buffer and incubated for 30-60 min on ice in the presence of 1 mL 10 mg/mL lysozyme, 20 µL 1 M $MgCl_2$, 20 µL 25 mg/mL DNase. Cells were lysed by sonication (25 cycles; 10 seconds pulse at 20% amplitude with 30 seconds off after each pulse) on ice, and the debris pelleted at 15000 rcf for 30 min. The supernatant was gently shaken with 2 mL Ni-NTA resin (Qiagen) pre-equilibrated with lysis buffer at 4 °C for 30-60 min in a plastic column. Unbound proteins were removed, and the resin washed with 15 mL lysis buffer, followed by 15 mL lysis buffer containing 10 mM Imidazole and finally with 15 mL lysis buffer containing 20 mM Imidazole. The His-tagged MurA was eluted with lysis buffer containing 300 mM imidazole. Buffers and eluted fractions were kept on ice. Elution fractions were combined and concentrated to 0.5 mL-1 mL using a vivaspin concentrator (5 kDa or 10 kDa M_W cutoff). The MurA variants were further purified by size-exclusion chromatography (SEC) on an AKTA FPLC equipped with a Superdex 200 10/300 GL SEC column. Samples were eluted with 1.5 column volumes of 50 mM Tris-HCl, 200 mM NaCl, pH 7.6 at 4 °C and a flow rate of 0.5 mL/min. Fractions containing monomeric MurA were pooled, concentrated and stored at -80 °C.

The S200 column was calibrated with blue dextran and protein standards (Sigma-Aldrich) consisting of carbonic anhydrase (29 kDa), albumin bovine serum (66 kDa), Amylase (200 kDa) and apoferritin (443 kDa), thyroglobulin (669 kDa).

Cleavage of the His-SUMO tag

For biophysical characterization, the His-SUMO tag was cleaved as follows. His-SUMO-MurA was partially denatured with 2 M urea by adding an equal volume of chilled denaturing buffer (50 mM Tris, 100 mM NaCl, 4 M urea, 2 mM DTT, pH 7.6). Next, ULP1 protease was added at a ratio of 1:100 (protease: MurA, by mass). After gentle manual mixing, the cleavage reaction was incubated overnight at 4 °C. The next day, the reaction was mixed with Ni-NTA resin pre-equilibrated with Tris-urea buffer (50 mM Tris, 150 mM NaCl, 2 M urea, 1 mM DTT pH 7.6) and shaken at 4 °C for 60 min. The flow-through containing MurA was collected and the Ni-NTA resin was washed with 15 mL Tris-urea buffer containing 10 mM and 20 mM Imidazole, respectively. The flow-through and wash fractions were combined and dialysed 2x against 1 L 50 mM Tris, 200 mM NaCl, 1 mM DTT at pH 7.6 at 4 °C. After dialysis, the protein solution was centrifuged at 15000 rcf, 4 °C for 30 min. The supernatant was concentrated using a vivaspin concentrator (5 kDa or 10 kDa M_W cutoff) to a final volume of 0.5 mL-1 mL and subsequently purified on a Superdex 200 column as described above. The fractions corresponding to monomeric MurA were collected and analysed on SDS-PAGE.

Quantification of isoAsp content by PIMT assay

isoAsp was quantified by measuring the amount of S-Adenosyl-l-homocysteine (AdoHcy) generated from the PIMT-catalysed methylation of isoAsp[21]. An AdoHcy standard curve was generated by injecting 60 µL of 0.25-5 µM AdoHcy onto an Agilent Zorbax 300SB-C18 column and eluting with a linear gradient of 0 to 30% acetonitrile (0.1% TFA) in water (0.1% TFA) at 50 °C and recording the absorbance at 260 nm. A plasmid encoding His_6-tagged human PIMT was obtained from Addgene (Catalog #34852). The protein was produced and purified by Ni-NTA chromatography under standard conditions.

Initial attempts to quantify isoAsp in MurA (2 µM) under native conditions were performed with 0.73 µM human PIMT. Optimized conditions to detect inaccessible isoAsp included a preincubation step in 3 M GdmCl at room temperature for 30-60 min. Other reaction components were then added to final concentrations of 2 µM MurA; 0.5

M GdmCl; 10 µM AdoMet; 14.6 µM human PIMT in 0.1 M NaPhos pH 6.8; 1 mM EDTA; 0.16% Triton. The reactions (100 µL total volume) were incubated for 30 min at 30 °C. Subsequently, the reaction was quenched by adding 20 µL 0.3 M phosphoric acid. 60 µL of the quenched reaction was injected to Agilent Zorbax 300SB-C18 column with a linear gradient of 0 to 30% acetonitrile at 50 °C. The amount of isoAsp in MurA variants was calculated from the absorbance of the AdoHcy peak at 260 nm based on an AdoHcy standard curve **(Figure S2)**. All AdoHcy peak areas were corrected based on a reaction conducted in the absence of substrate. Control peptides were included to verify the activity and specificity of PIMT under the assay conditions (sequence: SDLWKLLPEXNVLSPLPSQA, where X corresponds to either isoAsp or Asp).

Peptide mapping by LysC digest

LysC was dissolved into water to a final concentration of 1 mg/mL. 1 µL of the LysC solution was added to 20 µL 25 µM MurA in 50 mM Tris-HCl, 200 mM NaCl, pH 7.6 in an Eppendorf tube. The mixture was incubated at 37 °C for 21 h. After the incubation, 5 µL LC buffer C (water containing 0.1% formic acid) was added and the total 26 µL sample was transferred to a LC-MS vial. 10 µL (192 pmol) was injected for LC-MS analysis.

LC-MS analysis was conducted on a Waters Acquity UPLC CSH C18 1.7um, 2.1x150mm at 55 °C with a flow rate of 0.4 mL/min. The solvent system is water + 0.1% formic acid (solvent C) / acetonitrile + 0.1% formic acid (solvent D). The total run time was 45 min: 0-1.0 min (2% D); 1.0 – 29.0 min (2-45% D); 29.0-34.0 min (45-60% D); 34.0-35.0 min (60-95% D); 35.0-40.0 min (95-2% D); 40.0-45.0 min (2% D). The data was analysed on UNIFI and the coverage was 98% for MurA. The peaks corresponding to peptides encompassing residues 64-88 (VERXGSVWIDASNVNNFSAPYDLVK, where X is Asn, (iso)Asp or a succinimide) were further analysed by MS^E fragmentation. The following mass spectrometer settings were used: positive polarity, capillary voltage 3.0 kV, source temperature 120 °C, sampling cone 60 V, desolvation temperature 350 °C, *m/z* range 50 – 3000, transfer collision energy ramp 20 - 45 V.

Peptide mapping by AspN digest

AspN protease (New England Biolabs) was freshly reconstituted in pure water to a concentration of 1 mg/mL. 1 µL of the AspN solution was added to 20 µL 25 µM MurA in 50 mM Tris-HCl, 100 mM NaCl, 1 M Urea, 2.5 mM $ZnSO_4$, pH 7.6 in a PCR tube. The mixture was incubated at 36 °C for 21 h. After the incubation, 5 µL LC solvent C (water containing 0.1% formic acid) was added and the total 26 µL sample was transferred to a LC-MS vial. 5

µL was injected for LC-MS analysis. LC/MS and MS^E was performed as described for LysC-based peptide mapping. Peptides were automatically detected with UNIFI and manually analysed with masslynx.

Measurement of the rate of isoAsp formation in MurA

To enable measurement of the rate of isoAsp formation *in vitro*, MurA containing a high proportion of unmodified Asn67 was prepared ($MurA_{WT}$*). For this purpose, the production and purification procedure described above was accelerated as follows. MurA was produced in 200 mL batches with IPTG induction at 37 °C for 40-60 min. After expression, the culture was pelleted by centrifugation, resuspended in lysis buffer and lysed by sonication. The lysate was rapidly purified by Ni-NTA and size exclusion chromatography. The purified fractions from SEC were immediately aliquoted, flash-frozen with liquid N_2 and stored at -80 °C. The entire purification was carried out at 4 °C within 5-6 h to minimize isoAsp formation.

To measure the rate of isoAsp formation in MurA under native conditions, $MurA_{WT}$* (42.5 µM in 50 mM Tris-HCl, 200 mM NaCl, pH 7.6) was incubated at 37 °C in a PCR block and 12 µL aliquots removed at specified intervals. Samples were quenched by freezing and stored at -80 °C. The isoAsp content of all time points was measured in parallel using the PIMT assay under partially denaturing conditions as described above. To measure the rate of isoAsp formation in denatured MurA, $MurA_{WT}$* (42.5 µM in 50 mM Tris-HCl, 200 mM NaCl, pH 7.6) was mixed with an equal volume of 6 M GdmCl to reach a final GdmCl concentration of 3 M. Aliquots of the mixture were incubated at 37 °C and analyzed as above. Of note, MurA protein contains 13 Asn sites, two of which are followed by a glycine (Asn67 and Asn148) which likely deamidate with similar rates under denaturing conditions. The data was fit to the equation $Y = \mathrm{Y}_0 + \left(\mathrm{Y}_f - \mathrm{Y}_0\right) * (1 - e^{-kt})$.

The kinetics of isoAsp formation in the peptide $MurA_{63\text{-}73}$ were determined by the PIMT assay as described above or using a direct RP-HPLC method. For the former, aliquots of HPLC-purified peptide were dissolved in 50 mM Tris-HCl, 200 mM NaCl, pH 7.6 buffer to a concentration of 50 µM (determined by nanodrop), incubated at 37 °C and analyzed by the PIMT assay described above. Alternatively, peptides were dissolved in PBS buffer at a concentration of approximately 375 µM and incubated at 48, 55, 65 or 75 °C. Aliquots were removed and 20 µL analyzed by RP-HPLC using a PLRP-S column with 15%-40% B at 70 °C. The disappearance of the peak corresponding to the Asn-contain peptide was fit to an exponential decay (GraphPad Prism) and the half-life at 37 °C extrapolated using an Arrhenius plot.

MurA kinetics assay

MurA activity assays were performed in a 96 well plate at 37 °C for 10-15 min in a final volume of 150 µL reaction mixture containing 50 mM Tris-HCl-pH 7.5, 10 mM NaCl, 1 mM dithiothreitol (DTT), 0.6 mM UDP-GlcNAc (Sigma), and 44 nM of MurA variant. 1 mM Phosphoenolpyruvate (PEP, Sigma Aldrich) was added to initiate the reaction. The amount of inorganic phosphate (P_i) released was quantified by Malachite Green assay reagent (made in house) following the commercial supplier's protocol (Cayman Chemical Company, USA). Briefly, 150 µL of the reaction mixture were quenched by the addition of 30 µL reagent A. After subsequent addition of 30 µL reagent B, sample absorbance was measured at 620 nm using a multi-well plate reader. Absorbance was converted to [10] using a standard curve generated from phosphate standards. Initial velocities were calculated by linear regression. All rates were corrected for the background reaction in the absence of MurA.

To measure the K_m for UDP-GlcNAc, the above enzymatic assay was performed with different concentrations of UDP-GlcNAc (0 µM to 400 µM) at a fixed concentration of 1 mM PEP. The average velocity (µmol P_i/min) at each UDP-GlcNAc concentration was determined and $K_{m,app}$(UDP-GlcNAc) and $k_{cat,app}$ values were obtained by fitting the data to the Michaelis-Menten equation in GraphPad Prism.

***In vitro* aggregation assays**

In vitro aggregation of MurA variants was induced by incubation at low or high ionic strength, high temperature and/or low pH and monitored by analytical SEC. Stock solutions of 45 µM MurA in 50 mM Tris-HCl, 200 mM NaCl, pH 7.6 were diluted with four volumes of phosphate buffered saline (PBS) of varying compositions. Final conditions were: 150 mM NaCl, 10 mM Tris, 8 mM sodium phosphate, 2 mM KCl, pH 7.5 (normal); 1.6 M NaCl, 10 mM Tris, 8 mM sodium phosphate, 2 mM KCl, pH 7.5 (high salt); 40 mM NaCl, 10 mM Tris, 8 mM sodium phosphate, 2 mM KCl, pH 7.5 (low salt); 150 mM NaCl, 10 mM Tris, 8 mM sodium phosphate, 2 mM KCl, pH 6.0-6.2 (low pH). These samples were incubated as indicated, centrifuged, and injected onto an Agilent Advancebio SEC column (5 mL). Proteins were eluted with 50 mM Tris, 200 mM NaCl, pH 7.6 at a flow rate of 0.3 ml/min for 20 min. The recovery yield of proteins was calculated based on the area of monomeric MurA at a wavelength of 280 nm as compared to an untreated control sample. Measurements were conducted in triplicate.

To partially denature samples, MurA stock solutions in 50 mM Tris-HCl, 200 mM NaCl, pH 7.6 were diluted with an equal volume of 50 mM Tris-HCl, 100 mM NaCl, 2 mM DTT, 4 M urea. Samples in 2 M urea were incubated

for 3 h at room temperature, and then dialyzed in 1 L 50 mM Tris-HCl, 200 mM NaCl, 1 mM DTT, pH 7.6 overnight at 4 °C using a dialysis button. Amount of aggregation was estimated also by analytical size-exclusion chromatography.

CD spectroscopy

Far-UV CD spectra of protein samples were recorded at 25 °C on an Aviv 202 spectrometer from 270 nm to 200 nm in 1 nm steps with an averaging time of 1 s in 10 mM sodium phosphate, 150 mM NaCl, pH 7.6. MurA concentrations were 3.0 µM (1 mm cuvette) or 30 µM (0.1 mm cuvette). Two scans were averaged and a buffer blank was subtracted.

For chemical denaturation, the denaturation curve was obtained by measuring ellipticity of a 3 µM protein solution at 222 nm using a 1 mm cuvette, at urea concentrations between 0 and 9 M in 10 mM phosphate, 150 mM NaCl, pH 7.6 at 25 °C. The signal of each point was averaged over 1 min. Each urea concentration was diluted from a 10 M urea, 10 mM phosphate, 150 mM NaCl, pH 7.6 stock solution individually and the CD signal measured after 15 min equilibration time at 25 °C. The raw data from Aviv 202 software was fitted non-linearly to a two-state unfolding model with baseline correction using GraphPad Prism:

$Y = \frac{(\alpha_N + \beta_N[urea]) + (\alpha_D + \beta_D[\mathrm{urea}]) * e^{\frac{m_{D-N}([urea] - [\mathrm{urea}]_{50\%})}{RT}}}{1 + e^{\frac{m_{D-N}([urea] - [\mathrm{urea}]_{50\%})}{RT}}}$, where α_N and α_D are the CD signals of the native and denatured states, respectively. β_N and β_D are the slopes at low and high urea concentrations, respectively. Y is the raw CD signal, $m_{D\text{-}N}$ the cooperativity of unfolding and $D_{50\%}$ the denaturant concentration at which 50% of protein is unfolded.

Reversibility of chemical denaturation was assessed by measuring the kinetics of MurA denaturation and refolding. A 3 mL cuvette was used and protein concentration was 0.3 µM. Denaturation kinetics were measured at 25 °C immediately after diluting a protein stock to 3 mL with urea buffer (2 M Urea concentration); refolding kinetics were measured at 25 °C after incubating the protein in 300 µL 9 M urea buffer for 15 min at 25 °C and quickly diluting the solution to 2 M urea. Denaturation and refolding signals converged over time for both $MurA_{WT}$ and $MurA_{N67D}$. Under these conditions, refolding was >85% reversible for both variants (**Figure S3).**

A thermal denaturation curve was obtained by measuring ellipticity of a 1 µM protein solution at 222 nm between 4 °C and 95 °C. The sample was heated in 1 °C steps in 10 mM phosphate, 150 mM NaCl, pH 7.6 with 1 min equilibration time and 1 min signal averaging time per point. A 10 mm CD cuvette equipped with a stir bar was

used (total volume 3 mL). The fraction of folded MurA was calculated under the assumption that the unfolded fraction of the protein is 0 and 1 at 4 °C and 95 °C, respectively. An additional correction for temperature-specific change in CD signal was taken into account as follows. The data points from 4-30 °C and 80-95 °C were fit to a linear equation and extrapolated to reflect the folded $\theta_F(T)$ and unfolded $\theta_U(T)$ signal as a function of temperature. The fraction of unfolded protein at each temperature (F_U) is then calculated from the signal θ using the equation:

$$F_u = \frac{\theta - \theta_F(T)}{\theta_U(T) - \theta_F(T)}.$$

The melting temperatures were approximated through fitting the data to a 3-state model in GraphPad Prism using the equation:

$$F_U = \frac{F_I * e^{\Delta H_{m1}\left(\frac{T/T_{m1}-1}{RT}\right)} + e^{\Delta H_{m1}\left(\frac{T/T_{m1}-1}{RT}\right)} * e^{\Delta H_{m2}\left(\frac{T/T_{m2}-1}{RT}\right)}}{1+e^{\Delta H_{m1}\left(\frac{T/T_{m1}-1}{RT}\right)} + e^{\Delta H_{m1}\left(\frac{T/T_{m1}-1}{RT}\right)} * e^{\Delta H_{m2}\left(\frac{T/T_{m2}-1}{RT}\right)}},$$

where F_I is the contribution of the unfolding intermediate to the CD signal, R is the universal gas constant, T_{m1} and T_{m2} the melting temperatures for the first and second transition, and ΔH_{m1} and ΔH_{m2} the enthalpy of denaturation at the respective transition midpoint. A representative trace from 2 independent measurements is shown. In parallel, midpoints of transition were also determined from maxima of the first derivative of the thermal denaturation curve (after smoothing with a 2nd degree polynomial and 4 adjacent data points) in GraphPad Prism.

Analysis of MurA flexibility and solvent accessibility via HDX-MS

HDX-MS experiments[22] were carried out on a Synapt G2Si (Waters, UK) instrument coupled with a commercial HDX system (Waters, UK) and Acquity M-Class system. The instrument was calibrated with sodium iodide, run in sensitivity mode, MS^E fragmentation mode with electrospray ionization. The following mass spectrometer settings were used: positive polarity, capillary voltage 3.0 kV, source temperature 80 °C, sampling cone 30 V, desolvation temperature 200 °C, *m/z* range 50 – 2000, transfer collision energy ramp 25 - 45 V. Leucine enkephalin (Waters, UK) was used as the lockmass.

Stock solutions of $MurA_{WT}$ and $MurA_{N67D}$ were prepared at 20 µM. 5 µL of sample was diluted with 95 µL Buffer L (50 mM Tris-Hcl, 200 mM NaCl in deuterium oxide, pH 7.6) to initiate the HDX reaction and incubated for either 0.25, 1, 30 or 120 minutes in triplicate. 5 µL of sample was diluted with 95 µL Buffer E (50 mM Tris-Hcl, 200 mM NaCl, pH 7.6) for undeuterated references for 6 replicates. 70 µL of reaction mixture was quenched with 70 µL of quench solution (100 mM potassium phosphate, pH 2.3) at 1 °C. 100 µL of quenched sample was then injected

onto the HDX system. Samples were digested online with a Waters Enzymate BEH pepsin column at 20 °C and trapped on a Waters BEH C18 VanGuard column at 0 °C. Digestion and trapping was carried out for 3 minutes at 200 µL/min with 100% Mobile Phase A (0.2% formic acid). Peptides were eluted from the trapping column and separated on a Waters BEH C18 column (100 mm x 1.0 mm) at 0 °C over a 7-minute gradient of 8-40% Mobile Phase B (0.2% formic acid in acetonitrile) at 40 µL/min. All sample injections were followed with a clean blank with a saw-tooth gradient to prevent carryover. The pepsin column was cleaned with pepsin wash (1.5 M GdmCl, 4% acetonitrile, 0.8% formic acid) after each injection.

Peptides were identified using Waters ProteinLynx Global Server 2.5.1 (PLGS). Identified peptides were filtered and curated using Waters DynamX V3.0. Statistical analysis was performed using Deuteros v1.0 (King's College London, UK)[23] using a global confidence interval of 99%. Peptides were not corrected for back-exchange as absolute uptake is not required for differential HDX. Biological replicates were carried out to confirm the HDX results.

RESULTS

MurA features stoichiometric levels of isoAsp

Because of its biological importance[24] and the wealth of structural information[3], MurA represents an ideal test case to dissect potentially favorable roles of isoAsp in protein structure and function. To verify the presence and extent of the isoAsp modification in *E. cloacae* MurA we produced the enzyme in *E. coli* as an N-terminal fusion with a hexahistidine-SUMO tag (SUMO-$MurA_{WT}$). The resulting protein was purified by Ni-NTA affinity chromatography and gel filtration. The main peak in the size exclusion chromatogram corresponds to a monomer (**Figure S4a**, observed MW: 60 kDa, expected MW: 57 kDa). Approximately 10% of the protein eluted in the column void volume, presumably in the form of soluble aggregates. The monomer fraction contains pure MurA as judged by SDS PAGE (**Figure S5**) and the identity of the protein was confirmed by mass spectrometry (**Figure S6a**). To measure the extent of isoAsp modification in our preparation of SUMO-$MurA_{WT}$ we used a previously described enzymatic assay[25]. PIMT selectively methylates isoAsp using the cofactor S-Adenosyl methionine (AdoMet), concomitantly forming S-Adenosyl-L-homocysteine (AdoHcy) which is quantified by reverse phase (RP) HPLC. To our surprise, we observed only 3.5 ± 1.9 pmoles isoAsp per 100 pmoles of SUMO-$MurA_{WT}$ when the assay was performed under native conditions using catalytic amount of PIMT (**Figure 2a**). Under the same conditions, con-

trol peptides bearing an isoAsp or an Asp residue exhibited 93 ± 12 pmoles and 0.5 ± 0.1 pmoles isoAsp, respectively (**Figure 2a** and **Figure S4b**). Given that the relatively narrow active site of PIMT[26] is unlikely to accommodate folded proteins, we denatured MurA with 3M GdmCl prior to the PIMT assay and increased the concentration of PIMT during the assay. Under these conditions, stoichiometric amounts of isoAsp were detected (98 ± 3 pmoles, **Figure 2a, Figure S4c**). The near complete conversion to isoAsp as well as the requirement for MurA denaturation indicate that the isoAsp is embedded in a structural motif, consistent with isoAsp67 in several crystal structures[3, 27]. We speculate that the MurA fold also prevents access of PIMT to isoAsp67 *in vivo*.

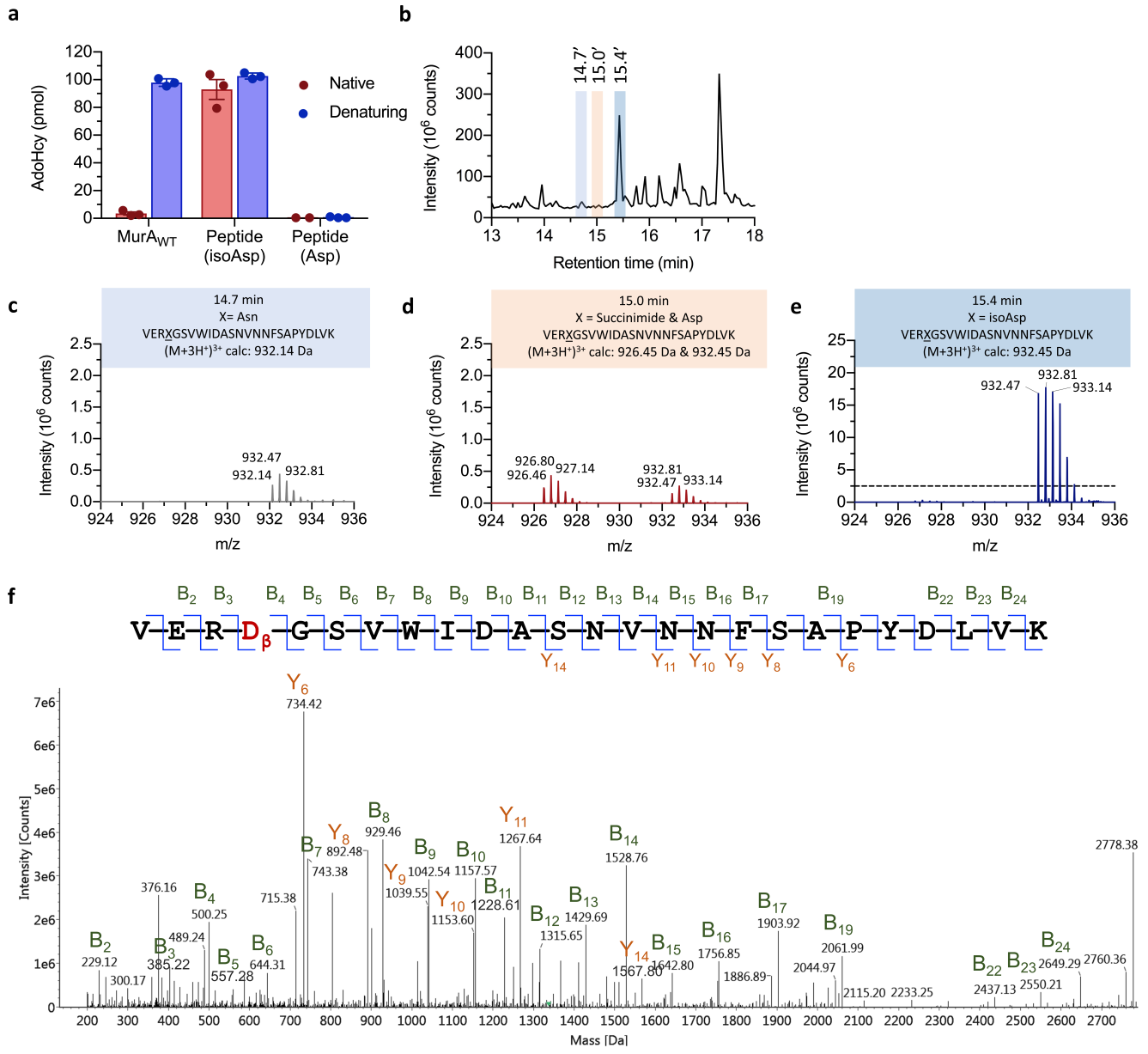

Figure 2: SUMO-MurA$_{WT}$ contains stoichiometric amounts of isoAsp. a *Biochemical determination of SUMO-MurA$_{WT}$ isoAsp content via PIMT-dependent methylation. 100 pmoles of SUMO-MurA$_{WT}$ or control peptides with or without an isoAsp*

residue are used as substrate. AdoHcy is quantified by RP-HPLC upon methylation of SUMO-MurA$_{WT}$ under native condition using catalytic amounts of PIMT (0.73 µM, red) or after pre-incubation with 3 M GdmCl and treatment with 14.6 µM PIMT (blue). ***b-f*** *Asn67 is fully deamidated.* ***b*** *LC-MS analysis of LysC digested MurA$_{WT}$. The peaks at 14.7 (**c**), 15.0 (**d**) and 15.4 (**e**) min correspond to peptide VERXGSVWIDASNVNNFSAPYDLVK (residues 64-88 in MurA), with X being Asn, succinimide & Asp and isoAsp respectively. The dashed line in* ***e*** *represents the scale of the spectra in* ***c*** *and* ***d****.* ***f*** *MS^E analysis of the 15.4 min peak from* ***e****. The masses of ions B$_3$ (calc: 385.22 Da, obs: 385.22 Da) and B$_4$ (calc: 500.25 Da, obs: 500.25 Da) confirm that X corresponds to an (iso)Asp residue.*

To further confirm the site of isoAsp formation we performed LC-MS analysis of LysC-digested MurA$_{WT}$ (**Figure 2b**). We detected several isoforms of the peptide corresponding to residues 64-88 (**Figure 2c-e**). Among these, the most intense peak (retention time 15.4 min, **Figure 2e**) exhibited a mass difference of +1 Da from the encoded sequence, indicating that, as expected, deamidation occurred. Based on the high isoAsp content determined in the PIMT assay, we assign the 15.4 min peak to the isoAsp67 form. Masses corresponding to the unmodified Asn sequence (retention time 14.7 min, **Figure 2c**) and a succinimide isoform (retention time 15.0 min, **Figure 2d**) were also present, albeit at 60-fold lower intensities. Fragmentation of the deamidated peak by MS^E analysis further confirmed the location of the deamidation at residue 67 (**Figure 2f**). Collectively, these results underscore that Asn67 has post-translationally isomerized to isoAsp to an extent of >95% in our preparations of MurA$_{WT}$.

The tertiary structure of MurA promotes rapid isoAsp formation

The presence of almost stoichiometric amounts of isoAsp at position 67 suggests that its formation is accelerated in MurA. We therefore sought to determine the rate of isomerization of this site *in vitro*. To access Asn67-containing MurA, we performed a rapid protein expression (1 h at 37 °C) and purification (~5 h at 4 ºC) of SUMO-MurA$_{WT}$. PIMT assays of flash-frozen aliquots from this preparation (MurA$_{WT}$*) revealed an isoAsp content of 22%, thus enabling a measurement of the rate of isoAsp formation. At 37 °C, MurA$_{WT}$* isomerizes with a half-life of 4.7 h, yielding >95% isoAsp content after 24 h (**Figure 3**). This rate is considerably faster than values for deamidation of Asn-Gly sequences measured in peptides (half-life ≈ 1d)[4] and estimated in proteins (mean half-life ≈ 100 days)[28]. Given the unusually high rate of isoAsp formation, we explored whether the structure of MurA facilitates this transformation. We incubated MurA$_{WT}$* at 37 °C in the presence of 3 M GdmCl to denature the protein. Under these conditions, isoAsp formation was >10x slower than under native conditions (half-life ≈ 80 h, **Figure**

3), which suggests that isoAsp formation in MurA is autocatalytic. Notably, the curve plateaus at approximately 200% isoAsp content under denaturing conditions. This observation is consistent with the presence of two Asn-Gly sequences in MurA (Asn67 and Asn148), which are expected to isomerize with similar rates in the unfolded protein. A synthetic peptide encompassing residues 63-73 ($MurA_{63-73}$) also isomerizes with a half-life ≈ 60 h (**Figure 3** and **Figure S7**), an order of magnitude slower than folded MurA. To further confirm this result, we determined the deamidation kinetics of the peptide $MurA_{63-73}$ at elevated temperatures directly by HPLC (**Figure S8**). An Arrhenius plot shows that the temperature dependence of the deamidation rate is linear, allowing extrapolation to 37°C (**Figure 3c**). The resulting half-life of ≈ 70 h is in good agreement with measurements using the PIMT assay (**Figure 3d**), further supporting the premise that the 3-dimensional structure of MurA is crucial for rapid isoAsp formation.

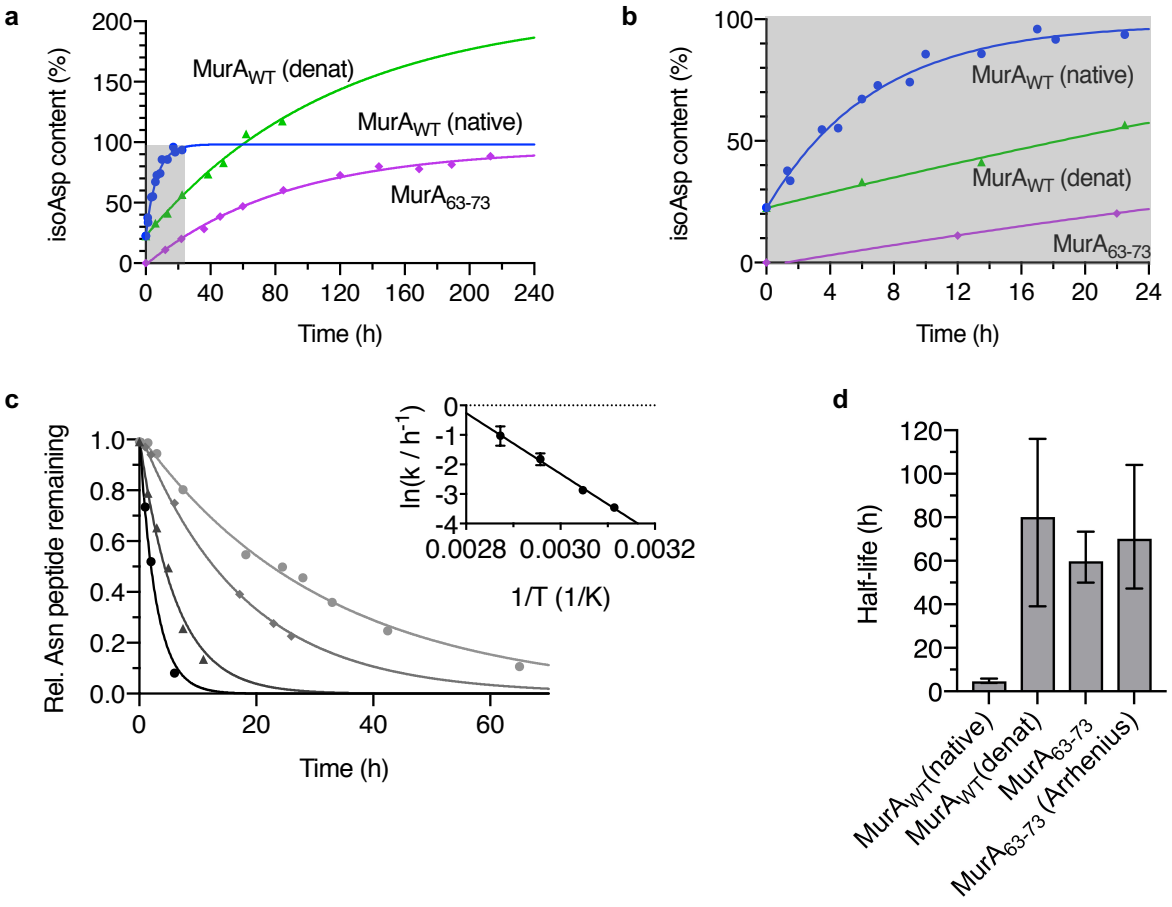

Figure 3: The 3D-structure of MurA facilitates Asn isomerization. ***a*** *Measurement of the isoAsp content of $MurA_{WT}$* after maturation at 37 °C under native (blue circles) and denaturing (3 M GdmCl, green triangles) conditions. Data points for $MurA_{WT}$* under native conditions are from two independent measurements. MurA contains two Asn-Gly sequences, expected to isomerize with similar rates under denaturing conditions. The isoAsp content of a peptide corresponding to residues 63-73 ($MurA_{63-73}$) is shown in pink diamonds.* ***b*** *Zoom-in for the initial 24 h period in* ***a*** *(shaded in grey).* ***c*** *Temperature dependence*

of $MurA_{63-73}$ deamidation measured by HPLC at 48, 55, 65 and 75 ºC. An Arrhenius plot is shown in the inset. ***d*** *Half-lives for isoAsp formation at 37 °C. Error bars represent the 95% CI of the fit from* ***a*** *and* ***c****.*

isoAsp67 improves the yield of recombinant MurA

The accelerated formation of stoichiometric isoAsp in MurA suggests that this backbone modification serves an important purpose. To address this hypothesis, we generated a series of MurA mutants and analyzed their properties. An Asn67Asp ($MurA_{N67D}$) mutation diminishes isoAsp formation at physiological pH and allows direct comparison between two variants with identical functional groups but distinct backbone connectivity. Mutations of the flanking residues Arg66 and Gly68 to Ala ($MurA_{R66A}$ and $MurA_{G68A}$, respectively) were introduced to probe their role in the isoAsp-containing beta hairpin. Arg66 contributes a salt bridge to the isoAsp α-carboxylate. The sterically minimal Gly68 is beneficial for rapid isoAsp formation; its mutation is expected to diminish isoAsp formation. All variants were produced in *E. coli* as His_6-SUMO fusions and purified by Ni-NTA chromatography and gel filtration. Strikingly, the mutants all exhibit considerable amounts of soluble aggregates and, accordingly, reduced yields of monomeric MurA (**Figure 4a**). This observation establishes that the isoAsp-containing hairpin is an important structural feature of MurA.

We isolated the monomeric fractions of the MurA mutants (see **Figure S5** and **Figure S6** for SDS-PAGE and mass spectra, respectively) and determined their isoAsp content (**Figure 4b**). SUMO-$MurA_{N67D}$ exhibited <5 % isoAsp which confirms that position 67 is indeed the predominant site of MurA isomerization. We further verified the modification state of residue 67 by peptide mapping. LC-MS analysis of LysC-digested $MurA_{WT}$ and $MurA_{N67D}$ revealed for each variant a predominant peak corresponding to residues 64-88 based on mass (**Figure S9**). Importantly, these isobaric peptides exhibited distinct retention times, as confirmed by co-injection (**Figure S9c**). Based on the total ion count for these peaks, we estimate that $MurA_{WT}$ contains >90% isoAsp. Conversely, $MurA_{N67D}$ exhibits predominantly Asp with approximately 10% isoAsp, slightly higher than determined via the PIMT assay. We did not detect additional isobaric peaks that could reflect the stereoisomers D-isoAsp and D-Asp, although their presence in small amounts cannot be excluded. To further validate this assignment, we performed a peptide mapping experiment with Asp-N (**Figure S10**) which cleaves N-terminal to Asp residues but cannot cleave isoAsp[29]. In $MurA_{WT}$, a peptide encompassing residues 51-72 was observed with a retention time of 13.5 min and a mass of 2490.3 Da (**Figure S10a, Figure S10c**). The signal for the same peptide was >10-fold lower in $MurA_{N67D}$ (**Figure S10b, Figure S10f**). By contrast, high-intensity peaks for peptides originating from cleavage

at Asp67 (residues 51-66: RT = 15.2 min, $M+H^+$ = 1834.0 Da and 67-72: RT = 13.6 min, $M+H^+$ = 676.3 Da) were observed in the mutant (**Figure S10g and Figure S10h**). These peaks were >100-fold lower in the wildtype (**Figure S10d Figure S10e**), further supporting the premise that residue 67 of the wildtype and the mutant are mostly isoAsp and Asp, respectively. As expected[4], the Gly to Ala mutation decelerates isoAsp formation in SUMO-$MurA_{G68A}$, with <30% of Asn67 being modified (**Figure 4b**). The $MurA_{R66A}$ mutant retained the ability to rapidly form isoAsp, demonstrating that Arg66 is not essential for this process.

We subsequently turned our attention to the catalytic activities of MurA variants. We quantified the phosphate released during MurA-catalyzed transfer of the enolpyruvyl moiety of PEP to UDP-GlcNAc[30]. Measurements of the initial velocities of MurA variants indicated that the activity of all mutant MurA were lower than the activity of the wild type, albeit only slightly (**Figure 4c**). The modest reduction in activity suggests that all variants retain the native MurA structure overall and is furthermore consistent with the location of isoAsp67 distal from the enzyme active site. To gain more insight into the nature of the reduction of activity, apparent $K_{m,app}$(UDP-GlcNAc) and $k_{cat,app}$ values of SUMO-$MurA_{WT}$ and SUMO-$MurA_{N67D}$ were determined at a constant concentration of PEP (1 mM) (**Figure 4d**). The $K_{m,app}$(UDP-GlcNAc) values were indistinguishable (97 μM and 103 μM for the isoAsp- and the Asp-containing variants, respectively, **Table 1**). By contrast, the $k_{cat,app}$ values differed by 20%-25%, with SUMO-$MurA_{WT}$ exhibiting the higher maximum velocity compared with the N67D mutant (**Table 1**). Thus, the lower activity of SUMO-$MurA_{N67D}$ is likely due to a reduced proportion of active enzyme, although subtle changes to the active site cannot be excluded.

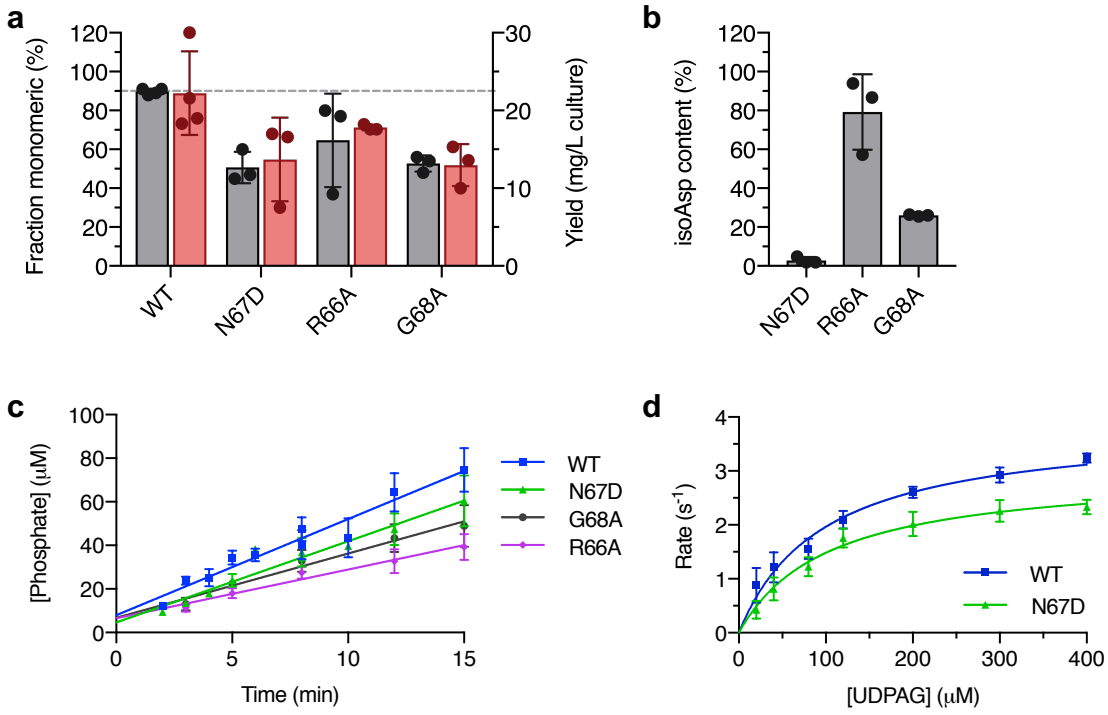

Figure 4: Characterization of MurA variants. a *Monomer fraction (grey, left axis) and yield (red, right axis) for SUMO-MurA variants after production and purification by Ni-NTA and size-exclusion chromatography (error bars: s.d. of four (WT) or three (mutants) biological replicates).* ***b*** *isoAsp-quantification for SUMO-MurA variants (error bars: s.d. of three biological replicates). The AdoHcy signals were corrected for the AdoHcy signal observed in a control reaction in the absence of substrate.* ***c*** *Relative activity measurement of SUMO-MurA variants (error bars: s.d. of four independent experiments).* ***d*** *Saturation kinetics of selected variants (error bars: s.d. of four independent experiments). Activities were recorded with 44 nM MurA variant, 1 mM PEP and 0.6 mM UDP-GlcNAc unless otherwise stated.*

Table 1: Kinetic characterization of MurA variants.

Variant*	**Relative activity (μM/min)***	**$k_{cat,app}$ (s^{-1})***	**$K_{m,app}$(UDP-GlcNAc) (μM)***	**$k_{cat,app}/K_{m,app}$ ($mM^{-1}s^{-1}$)**
SUMO-$MurA_{WT}$	4.4 ± 0.3	3.9 ± 0.19	97 ± 13	40 ± 8
SUMO-$MurA_{N67D}$	3.7 ± 0.3	3.0 ± 0.15	103 ± 14	29 ± 6
SUMO-$MurA_{R66A}$	2.2 ± 0.2	-	-	-
SUMO-$MurA_{G68A}$	3.0 ± 0.3	-	-	-

** Ranges represent the errors of the fit from data shown in* ***Figure 4****.*

isoAsp67 reduces aggregation of MurA under stress conditions

Given that MurA variants with mutations in the isoAsp loop readily aggregate during protein production or purification from *E. coli* lysate, we sought to investigate MurA aggregation vulnerability in a more controlled way *in vitro*. We performed these measurements with $MurA_{WT}$ and $MurA_{N67D}$ mutant upon removal of the His-SUMO tag with Ulp1 protease, followed by size-exclusion chromatography. The cleaved variants were judged as pure by SDS-PAGE and mass spectrometry (**Figure S5, Figure S11** and **Figure S12**). Circular dichroism spectroscopy and native ion mobility mass spectrometry indicate that $MurA_{WT}$ and $MurA_{N67D}$ mutant have similar secondary structure and overall shape (**Figure S13**), confirming that their folds are the same.

The two variants were subjected to various stress conditions and their quaternary structures analyzed by size exclusion chromatography. Specific challenges included high temperature (42 °C and 47 °C vs 37 °C), low pH (pH 6.0 vs 7.5), extreme salt concentrations (1.6 M and 40 mM vs 150 mM NaCl) and combinations thereof. Of note, for both MurA variants the isoelectric point is pI = 5.7. After incubation at 37 °C overnight, both variants retained their monomeric state when exposed to low and high concentrations of NaCl or low pH (**Figure 5a**, **Figure S14a, Figure S14b**). Upon treatment at 42 °C overnight or 47 °C for 1 h, however, $MurA_{N67D}$ aggregated under otherwise ambient conditions (45 ± 5 % monomeric, **Figure 5a**, **Figure S14c, Figure S14d**). Aggregation was exacerbated under low salt conditions (22 ± 3% monomeric) as well as at low pH (<10 % monomeric) but diminished in the presence of 1.6 M NaCl. The isoAsp linkage clearly provides a protective effect under heat shock treatment, with more than 50% of $MurA_{WT}$ retaining its monomeric form under all conditions tested (**Figure 5a**). Partial denaturation with 2 M urea for 3 h, followed by renaturation by dialysis into native buffer, also resulted in the formation of approximately 80% aggregate for $MurA_{N67D}$ and only 20% for $MurA_{WT}$ (**Figure 5b**, **Figure S14e**). Collectively, these results suggest that the unusual isoAsp-containing hairpin plays an important role in maintaining the structural integrity of *Enterobacterial* MurA under stress conditions.

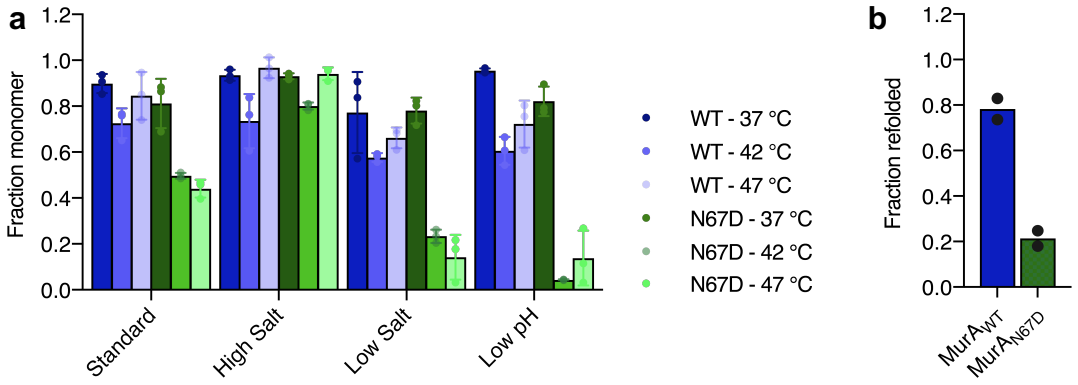

Figure 5: isoAsp formation improves MurA resilience against stress conditions. a *Relative recovery of monomeric MurA$_{WT}$ and MurA$_{N67D}$ after incubation at non-optimal temperatures, pH and salt concentrations. Standard conditions: 150 mM NaCl, 10 mM Tris, 8 mM sodium phosphate, 2 mM KCl, pH 7.5; High salt: standard conditions with 1.6 M NaCl; Low salt: Standard conditions with 40 mM NaCl; Low pH: standard conditions with pH = 6.0-6.2 (error bars: s.d. of three independent experiments).* ***b*** *Refolding yield upon partial denaturation with urea. MurA$_{WT}$ and MurA$_{N67D}$ were incubated in 2 M urea for 3 h at room temperature and subsequently dialyzed overnight at 4 °C.*

The stability of MurA variants was further explored by chemical and thermal denaturation. Circular dichroism spectroscopy (CD) revealed that both variants unfold cooperatively in the presence of urea (**Figure 6a, Figure S3**). Based on a 2-state model[31], the urea concentrations required to unfold 50% of MurA$_{WT}$ and MurA$_{N67D}$ are 2.6 M and 2.0 M, respectively. These values indicate that MurA$_{WT}$ is more resilient against chemical denaturation. However, the different cooperativities of unfolding ($m_{D\text{-}N}$ = 5.1 ± 0.3 and 8.6 ± 0.9 kJ/mol/M for MurA$_{WT}$ and MurA$_{N67D}$, respectively) preclude a quantitative comparison of the free energy of unfolding. Thermal denaturation experiments confirmed that MurA$_{WT}$ unfolds cooperatively with an apparent midpoint of thermal unfolding at 58.5 °C (**Figure 6b**). Inspection of the first derivative of the thermal unfolding curve suggests the presence of an unfolding intermediate, indicated by a small shoulder at 53.0 °C (**Figure 6c**). This intermediate is much more pronounced for MurA$_{N67D}$, which clearly exhibits two distinct transitions at 49.5 °C and 60.5 °C (**Figure 6b,c**). We thus conclude that isoAsp67 stabilizes MurA by preventing partial unfolding at lower temperatures.

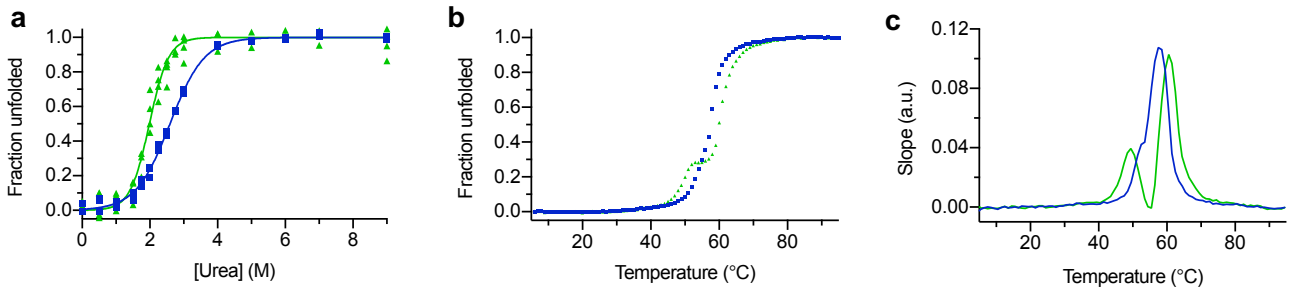

Figure 6: isoAsp67 impacts the stability of MurA. a *Chemical denaturation of $MurA_{WT}$ (blue squares) and $MurA_{N67D}$ (green triangles). The fraction unfolded was calculated from the circular dichroism signal at 222 nm. CD signals were recorded in the presence of 0 – 9 M urea at a protein concentration of 3 µM at 25 °C in a 1 mm cuvette. Unfolding curves are fit to the equation* $Y = \frac{(\alpha_N + \beta_N[urea]) + (\alpha_D + \beta_D[urea]) * e^{\frac{m_{D-N}([urea]-[urea]_{50\%})}{RT}}}{1 + e^{\frac{m_{D-N}([urea]-[urea]_{50\%})}{RT}}}$*, where* $m_{D\text{-}N}$ *is the cooperativity of unfolding and* $[urea]_{50\%}$ *is the denaturant concentration at which 50% of the protein is unfolded*[32]*. Individual data points from three ($MurA_{WT}$) and four ($MurA_{N67D}$) experiments are shown after correction for baseline slopes and calculation of the fraction unfolded at each [urea].* ***b*** *Thermal denaturation of $MurA_{WT}$ (blue squares) and $MurA_{N67D}$ (green triangles). A representative plot from two independent measurements is shown. CD signals at 222 nm were recorded at a protein concentration of 1 µM between 4 °C and 95 °C at 1 °C intervals using a 1 cm cuvette.* ***c*** *Slope of the thermal denaturation curve. The first derivative from the curves in* ***b*** *were calculated after smoothing the denaturation curve with a 2nd degree polynomial and 4 adjacent data points.*

Mutation of isoAsp67 causes local unfolding

We sought to gain structural insights into how isoAsp protects MurA from partial unfolding and aggregation with hydrogen-deuterium exchange mass spectrometry (HDX-MS). The technique measures the solvent exchange rate of backbone amide hydrogens in proteins, and thereby provides a measure of local structural changes and protein dynamics[33, 34]. Here we used HDX, followed by on-column pepsin digestion and LC-MS[35] to measure the dynamics of $MurA_{WT}$ and $MurA_{N67D}$. We compared differential exchange regimes ranging from 0.25 min to 2 hrs. Peptides within the regions of residues ~40-55 and ~55-70 exhibited increased deuterium uptake in the mutant $MurA_{N67D}$ as compared to $MurA_{WT}$ (**Figure 7a,b**, **Figure S15**). Such local changes in dynamics for the latter (residues ~55-70, **Figure 7d**) were expected given that this region encompasses the isoAsp67-containing hairpin in $MurA_{WT}$. The preceding region (~40-55, **Figure 7c**), which also becomes more dynamic upon mutation of isoAsp67, corresponds to an amphiphilic helix and a connected loop which pack against the isoAsp-containing hairpin toward the protein interior. Thus, the HDX-MS experiments demonstrate that altering the unique connectivity

of isoAsp through an N67D mutation increases local unfolding of the hairpin which propagates to neighboring structural elements on a timescale of minutes to hours.

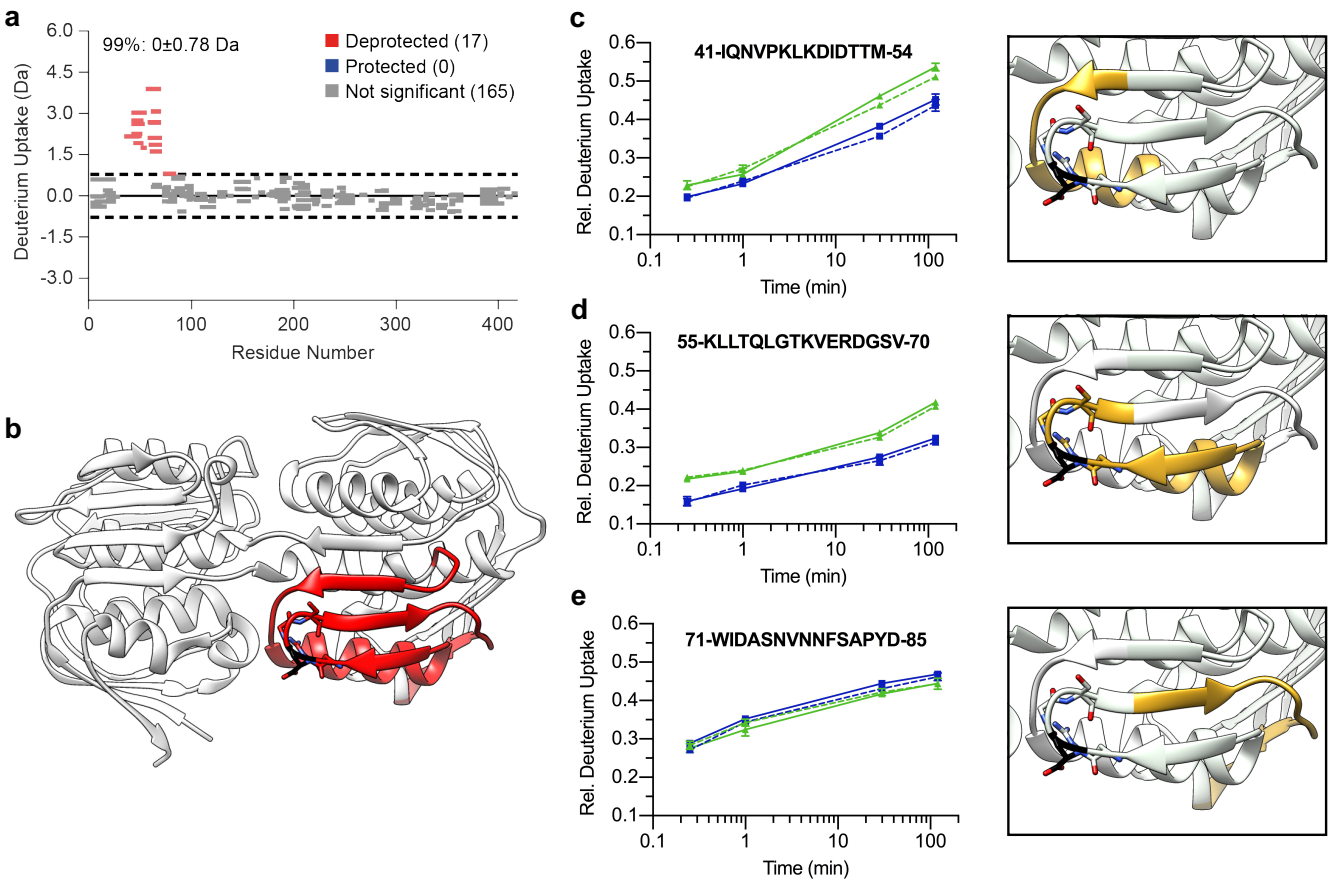

Figure 7: HDX-MS analysis of MurA structure and dynamics. a *Difference of deuterium uptake between* $MurA_{N67D}$ *and* $MurA_{WT}$*. Woods plots (exposure time sums) from two biological replicates are combined. The dashed line corresponds to a 99% confidence interval. Mutation of isoAsp67 significantly increases the deuterium uptake between residues 41-55 and 55-71.* ***b*** *Regions of MurA displaying significantly enhanced deuterium uptake in* $MurA_{N67D}$ *as compared to* $MurA_{WT}$ *are coloured in red and mapped onto the structure of MurA (pdb: 1ejc).* ***c-e*** *Deuterium uptake plots of peptides surrounding residues 67 of* $MurA_{WT}$ *(blue squares) and* $MurA_{N67D}$ *(green triangles). The location of the corresponding peptides within the structure of MurA is shown in golden (right panels). Two biological replicates were recorded (solid and dashed lines) with three technical replicates each (error bars: s.d.).*

DISCUSSION

Post translational backbone modifications are pervasive and play an important yet underappreciated role in protein biochemistry[36]. The rearrangement of Asn residues to β-Asp linkages is widely acknowledged to be involved

in ageing and damage of proteins, and is thought to be the culprit for biological abnormalities[8, 13, 14]. Furthermore, the formation of isoAsp has been found to cause adverse immune reactions[37] and negatively impact therapeutic proteins[38] including monoclonal antibodies[39, 40]. In stark contrast to such adverse effects, our work shows that the spontaneous formation of isoAsp in the β-hairpin of MurA from *Enterobacter cloacae* is beneficial. Remarkably, isoAsp formation was accelerated by an order of magnitude in folded MurA and yields isoAsp in an unusually homogeneous fashion. These observations suggest that the 3D structure of MurA enhances the formation of the succinimide intermediate as well as its regioselective hydrolysis, which supports the notion that MurA has evolved to exploit this residue. In agreement with this hypothesis, we found that perturbation of the isoAsp-containing hairpin by mutagenesis led to extensive aggregation during production and purification as well as under controlled stress conditions *in vitro*. Through biophysical analysis via HDX-MS we have pinpointed that replacement of the isoAsp with Asp causes local changes in dynamics and destabilizes nearby structural elements. Such local unfolding likely reveals hydrophobic surfaces which promote aggregation.

To understand the potential structural role of isoAsp it is instructive to compare the hairpin of MurA to a typical Type II' β-hairpin[41] (**Figure 8a**). Because Arg66 (φ=-137°,ψ=172°) and Ser69 (φ=-103°,ψ=167°) adopt a conformation compatible with β-sheet formation we consider them as flanking the hairpin. In terms of position and conformation (φ=-67°,ψ=-21°), Gly68 takes the place of hairpin residue i+2. isoAsp67 spans the distance covered by hairpin residues i and i+1. An H-bond between the isoAsp backbone NH and the C=O of Ser69 (3.1 Å from N to O) results in a 12-membered H-bonded ring. In Type II' β-hairpins, the similarly placed NH of residue i and C=O of i+3 form a 14-membered H-bonded ring. The additional methylene group within the backbone of isoAsp enables this extra range at a minimal entropic cost given that the dihedral angle θ is 62° (N-Cα-Cβ-CO), a value that is almost ideal for the sp^3-sp^3 centers present in *β*-amino acids[16, 42]. Another unique feature of isoAsp is the position of the α-carboxy group, which points in a direction otherwise only accessible to D-amino acids. This arrangement enables a salt bridge between isoAsp67 and Lys46 (**Figure 8b**). Indeed, our HDX-MS results are consistent with such an interaction, where the isoAsp-containing hairpin serves as a 'lid' to stabilize a helix adjacent to Lys46.

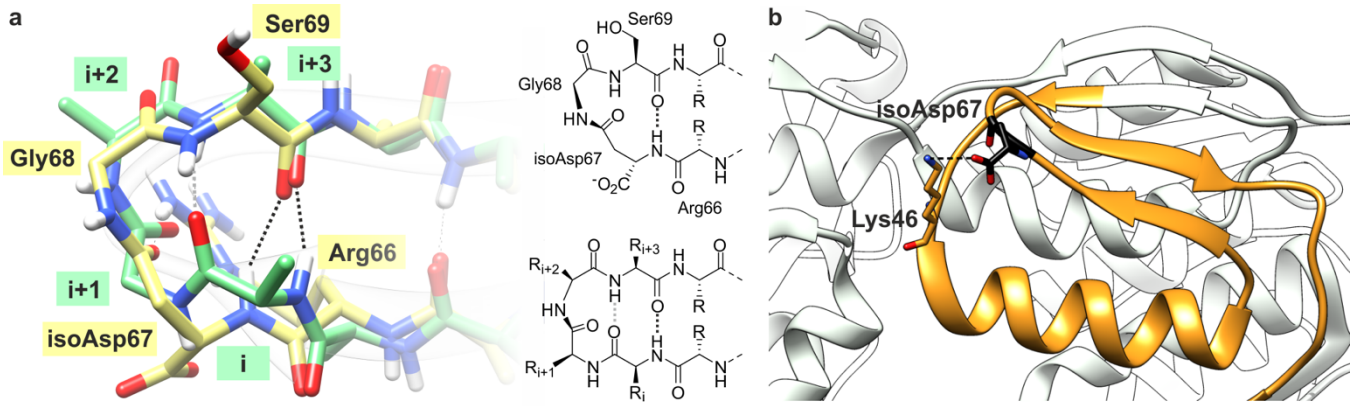

***Figure 8: isoAsp enables the formation of an unusual β-hairpin**. **a** Comparison of the isoAsp-containing β-hairpin of MurA from E. cloacae (4e7b, yellow) with a typical Type II' turn (1uxa, green). H-bonds are indicated by dashed lines. The backbone atoms of a 12- and 14-membered H-bonded ring are indicated for MurA (NH of isoAsp67 to CO of Ser69) and the Type II' turn (NH of i to CO of i+3), respectively. A 10-membered H-bonded ring of the Type II' turn (CO of i to NH of i+3) is shown in gray. ChemDraw structures of the turns are shown on the right (MurA: top, Type II': bottom). **b** The α-carboxylate of isoAsp67 interacts with Lys46 (dashed line, O-N distance = 3.35Å).*

Investigations on the effect of artificially introduced *β*-amino acids have established that expansion of the peptide backbone by an additional methylene group is tolerated in many structural contexts[43-45], including helices[46], sheets[47], turns[48-50] and even within an enzyme active site[51]. In most cases, such synthetic backbone expansions lead to small losses in stability. Judicious choice of the site and residue can, however, result in hairpins which improve the stability of select proteins, for example RNAse A[49] and the Pin1 WW domain[52]. The configurations of these artificial hairpins are distinct from the naturally occurring hairpin of MurA; whether the latter structure could similarly stabilize other proteins remains unexplored.

Other spontaneous protein backbone modifications have previously been shown to be beneficial for protein structure and function. The most prominent example is the fluorescent protein GFP from the jellyfish *Aequorea victoria*. In the process of establishing the fluorophore core of GFP, the three amino acids Thr-Tyr-Gly will undergo a series of backbone PTMs, including backbone cyclization, dehydration, and oxidation[53]. The methylene imidazolone (MIO) cofactor of amino mutases is established in a similar manner[54]. More recently, glutaminase from the hyperthermophilic archaeon *Methanocaldoccocus jannaschii* has been shown to contain a stable succinimide, shielded from hydrolysis by surrounding residues[55]. This unusual residue contributes to the extraordinary stability of glutaminase by rigidifying its surroundings[55]. Similarly, a succinimide residue has been shown to contribute to

the substrate recognition of amylomaltase[56]. Our results demonstrate that nature similarly exploits isoAsp formation to access unusual structures and thereby tailor protein structure and function. This mode of action may be enhanced by the possibility of enzymatic isoAsp formation[57, 58] and complements previously studied systems where slow asparagine deamidation and/or isoAsp accumulation regulates biochemical function[2]. Examples include apoptosis[59, 60], cell adhesion[61], host recognition[62] as well as the potential for modulation of transcription and translation through molecular ageing of histones[63] and ribosomes[64]. The continued discovery of proteins featuring isoAsp or succinimide linkages, as well as the ease in which MurA incorporates and utilizes its isoAsp residue highlights that such backbone modifications contribute favorably to the structural diversity of proteins. Hence, we speculate that isoAsp-containing hairpins are more common than anticipated and that their stabilizing effects could be harnessed in protein engineering efforts.

ASSOCIATED CONTENT

SUPPLEMENTARY INFORMATION

Figure S1- S15

Accession code (Uniprot code): P33038

AUTHOR INFORMATION

CORRESPONDING AUTHOR

*manuel.muller@kcl.ac.uk

AUTHOR CONTRIBUTIONS

M.M.M conceived the project; T.Z., K.H., A.P. and M.M.M. designed research and analysed data; T.Z. and K.H. performed experiments with guidance from A.P. and M.M.M. All authors contributed to the writing of the manuscript.

NOTES

The authors declare that they have no conflict of interest.

ACKNOWLEDGMENTS

This work was supported by the Wellcome Trust and the Royal Society (Sir Henry Dale Fellowship 202250/Z/16/Z to M.M.M), Waters Corporation (Grant to A.P.), China Scholarship Council (Studentship to T.Z.), and the London Interdisciplinary Doctoral Programme, Waters & King's College London for funding to K.H. The authors thank

Ernst Schönbrunn for providing the *Enterobacter cloacae* MurA plasmid; Dr Heather Findlay and Dr Nicola Harris for advice on CD spectroscopy; Dr Camille Metier for providing malachite green molybdate reagents; King's College London Chemistry Department Facility, Dr. Katia Grira, Dr. Steven Howell and Dr. Bram Snijders for advice with mass spectrometry; all members of the Müller lab for helpful discussions.

REFERENCES:

[1] Reissner, K. J., and Aswad, D. W. (2003) Deamidation and isoaspartate formation in proteins: unwanted alterations or surreptitious signals?, *Cell. Mol. Life Sci. 60*, 1281-1295.

[2] Robinson, N. E., and Robinson, A. (2004) *Molecular clocks: deamidation of asparaginyl and glutaminyl residues in peptides and proteins*, Althouse Press.

[3] Eschenburg, S., and Schonbrunn, E. (2000) Comparative X-ray analysis of the un-liganded fosfomycin-target MurA, *Proteins 40*, 290-298.

[4] Robinson, N. E., and Robinson, A. B. (2001) Molecular clocks, *Proc. Natl. Acad. Sci. U S A 98*, 944-949.

[5] Xie, M., and Schowen, R. L. (1999) Secondary Structure and Protein Deamidation, *J. Pharm. Sci. 88*, 8-13.

[6] Shimizu, T., Matsuoka, Y., and Shirasawa, T. (2005) Biological Significance of Isoaspartate and Its Repair System, *Biol. Pharm. Bull. 28*, 1590-1596.

[7] Fukuda, H., Shimizu, T., Nakajima, M., Mori, H., and Shirasawa, T. (1999) Synthesis, aggregation, and neurotoxicity of the alzheimer's Aß1-42 amyloid peptide and its isoaspartyl isomers, *Bioorg. Med. Chem. Lett. 9*, 953-956.

[8] Shimizu, T., Watanabe, A., Ogawara, M., Mori, H., and Shirasawa, T. (2000) Isoaspartate formation and neurodegeneration in Alzheimer's disease, *Arch. Biochem. Biophys. 381*, 225-234.

[9] Warmack, R. A., Boyer, D. R., Zee, C.-T., Richards, L. S., Sawaya, M. R., Cascio, D., Gonen, T., Eisenberg, D. S., and Clarke, S. G. (2019) Structure of amyloid-β (20-34) with Alzheimer's-associated isomerization at Asp23 reveals a distinct protofilament interface, *Nat. Commun. 10*, 3357.

[10] Lampi, K. J., Wilmarth, P. A., Murray, M. R., and David, L. L. (2014) Lens β-crystallins: the role of deamidation and related modifications in aging and cataract, *Prog. Biophys. Mol. Biol. 115*, 21-31.

[11] McFadden, P. N., and Clarke, S. (1987) Conversion of isoaspartyl peptides to normal peptides: implications for the cellular repair of damaged proteins, *Proc. Natl. Acad. Sci. U S A 84*, 2595-2599.

[12] Johnson, B. A., Murray, E. D., Clarke, S., Glass, D. B., and Aswad, D. W. (1987) Protein carboxyl methyltransferase facilitates conversion of atypical L-isoaspartyl peptides to normal L-aspartyl peptides, *J. Biol. Chem. 262*, 5622-5629.

[13] Lowenson, J. D., Kim, E., Young, S. G., and Clarke, S. (2001) Limited Accumulation of Damaged Proteins in L-Isoaspartyl (D-Aspartyl) O-Methyltransferase-deficient Mice, *J. Biol. Chem. 276*, 20695-20702.

[14] Yamamoto, A., Takagi, H., Kitamura, D., Tatsuoka, H., Nakano, H., Kawano, H., Kuroyanagi, H., Yahagi, Y.-i., Kobayashi, S.-i., Koizumi, K.-i., Sakai, T., Saito, K.-i., Chiba, T., Kawamura, K., Suzuki, K., Watanabe, T., Mori, H., and Shirasawa, T. (1998) Deficiency in Protein Isoaspartyl Methyltransferase Results in a Fatal Progressive Epilepsy, *J. Neurosci. 18*, 2063-2074.

[15] Heijenoort, J. v. (2001) Recent advances in the formation of the bacterial peptidoglycan monomer unit, *Nat. Prod. Rep. 18*, 503-519.

[16] Seebach, D., Beck, A. K., and Bierbaum, D. J. (2004) The World of β- and γ-Peptides Comprised of Homologated Proteinogenic Amino Acids and Other Components, *Chem. Biodiv. 1*, 1111-1239.

[17] Gellman, S. H. (1998) Foldamers: A manifesto, *Acc. Chem. Res. 31*, 173-180.

[18] Minasov, G., Halavaty, A., Filippova, E. V., Shuvalova, L., Dubrovska, I., Winsor, J., Papazisi, L., and Anderson, W. F. (2011) 2.6 Angstrom Crystal Structure of UDP-N-acetylglucosamine 1-carboxyvinyltransferase 1 (MurA1) from Bacillus anthracis. 10.2210/pdb3SG1/pdb.

[19] Yoon, H. J., Lee, S. J., Mikami, B., Park, H. J., Yoo, J., and Suh, S. W. (2008) Crystal structure of UDP-N-acetylglucosamine enolpyruvyl transferase from *Haemophilus influenzae* in complex with UDP-N-acetylglucosamine and fosfomycin, *Proteins 71*, 1032-1037.

[20] Minasov, G., Shuvalova, L., Dubrovska, I., Kiryukhina, O., Grimshaw, S., Kwon, K., and Anderson, W. F. (2017) 2.0 Angstrom Resolution Crystal Structure of UDP-N-acetylglucosamine 1-carboxyvinyltransferase from Streptococcus pneumoniae in Complex with Uridine-diphosphate-2(n-acetylglucosaminyl) butyric acid, (2R)-2-(phosphonooxy)propanoic acid and Magnesium. 10.2210/pdb5WI5/pdb.

[21] Schurter, B. T., and Aswad, D. W. (2000) Analysis of isoaspartate in peptides and proteins without the use of radioisotopes, *Anal. Biochem. 282*, 227-231.

[22] Masson, G. R., Burke, J. E., Ahn, N. G., Anand, G. S., Borchers, C., Brier, S., Bou-Assaf, G. M., Engen, J. R., Englander, S. W., Faber, J., Garlish, R., Griffin, P. R., Gross, M. L., Guttman, M., Hamuro, Y., Heck, A. J. R., Houde, D., Iacob, R. E., Jorgensen, T. J. D., Kaltashov, I. A., Klinman, J. P., Konermann, L., Man, P., Mayne, L., Pascal, B. D., Reichmann, D., Skehel, M., Snijder, J., Strutzenberg, T. S., Underbakke, E. S., Wagner, C., Wales, T. E., Walters, B. T., Weis, D. D., Wilson, D. J., Wintrode, P. L., Zhang, Z., Zheng, J., Schriemer, D. C., and Rand, K. D. (2019) Recommendations for performing, interpreting and reporting hydrogen deuterium exchange mass spectrometry (HDX-MS) experiments, *Nat. Methods 16*, 595-602.

[23] Lau, A. M. C., Ahdash, Z., Martens, C., and Politis, A. (2019) Deuteros: software for rapid analysis and visualization of data from differential hydrogen deuterium exchange-mass spectrometry, *Bioinformatics 35*, 3171-3173.

[24] Brown, E. D., Vivas, E. I., Walsh, C. T., and Kolter, R. (1995) MurA (MurZ), the enzyme that catalyzes the first committed step in peptidoglycan biosynthesis, is essential in Escherichia coli, *J. Bacteriol. 177*, 4194-4197.

[25] Johnson, B. A., and Aswad, D. W. (1991) Optimal conditions for the use of protein L-isoaspartyl methyltransferase in assessing the isoaspartate content of peptides and proteins, *Anal. Biochem. 192*, 384-391.

[26] Griffith, S. C., Sawaya, M. R., Boutz, D. R., Thapar, N., Katz, J. E., Clarke, S., and Yeates, T. O. (2001) Crystal structure of a protein repair methyltransferase from *Pyrococcus furiosus* with its L-isoaspartyl peptide substrate, *J. Mol. Biol 313*, 1103-1116.

[27] Bensen, D. C., Rodriguez, S., Nix, J., Cunningham, M. L., and Tari, L. W. (2012) Structure of MurA (UDP-N-acetylglucosamine enolpyruvyl transferase) from *Vibrio fischeri* in complex with substrate UDP-N-acetylglucosamine and the drug fosfomycin, *Acta. Cryst. F 68*, 382-385.

[28] Robinson, N. E. (2002) Protein deamidation, *Proc. Natl. Acad. Sci. USA 99*, 5283-5288.

[29] Shujia, D., David, H. L., Nathaniel, T. K., and Zhaohui, S. Z. (2013) Peptidyl-Asp Metalloendopeptidase, In *Handbook of Proteolytic Enzymes*, pp 1281-1285.

[30] Lanzetta, P. A., Alvarez, L. J., Reinach, P. S., and Candia, O. A. (1979) An improved assay for nanomole amounts of inorganic phosphate, *Anal. Biochem. 100*, 95-97.

[31] Clarke, J., and Fersht, A. R. (1993) Engineered disulfide bonds as probes of the folding pathway of barnase: increasing the stability of proteins against the rate of denaturation, *Biochemistry 32*, 4322-4329.

[32] Fersht, A. (1999) *Structure And Mechanism in Protein Science*, W. H. Freeman and Company.

[33] Engen, J. R. (2009) Analysis of protein conformation and dynamics by hydrogen/deuterium exchange MS, *Anal. Chem. 81*, 7870-7875.

[34] Konermann, L., Pan, J., and Liu, Y. H. (2011) Hydrogen exchange mass spectrometry for studying protein structure and dynamics, *Chem. Soc. Rev. 40*, 1224-1234.

[35] Martens, C., Shekhar, M., Borysik, A. J., Lau, A. M., Reading, E., Tajkhorshid, E., Booth, P. J., and Politis, A. (2018) Direct protein-lipid interactions shape the conformational landscape of secondary transporters, *Nat. Commun. 9*, 4151.

[36] Müller, M. M. (2018) Post-Translational Modifications of Protein Backbones: Unique Functions, Mechanisms, and Challenges, *Biochemistry 57*, 177-185.

[37] Mamula, M. J., Gee, R. J., Elliott, J. I., Sette, A., Southwood, S., Jones, P.-J., and Blier, P. R. (1999) Isoaspartyl Post-translational Modification Triggers Autoimmune Responses to Self-proteins, *J. Biol. Chem. 274*, 22321-22327.

[38] Manning, M. C., Chou, D. K., Murphy, B. M., Payne, R. W., and Katayama, D. S. (2010) Stability of Protein Pharmaceuticals: An Update, *Pharm. Res. 27*, 544-575.

[39] Yokoyama, H., Mizutani, R., Noguchi, S., and Hayashida, N. (2019) Structural and biochemical basis of the formation of isoaspartate in the complementarity-determining region of antibody 64M-5 Fab, *Sci. Rep. 9*.

[40] Jefferis, R. (2016) Posttranslational Modifications and the Immunogenicity of Biotherapeutics, *J. Immunol. Res 2016*, 5358272-5358272.

[41] de Brevern, A. G. (2016) Extension of the classical classification of β-turns, *Sci. Rep. 6*, 33191.

[42] Chatterjee, S., Roy, R. S., and Balaram, P. (2007) Expanding the polypeptide backbone: hydrogen-bonded conformations in hybrid polypeptides containing the higher homologues of alpha-amino acids, *J. R. Soc. Interface 4*, 587-606.

[43] George, K. L., and Horne, W. S. (2018) Foldamer Tertiary Structure through Sequence-Guided Protein Backbone Alteration, *Acc. Chem. Res. 51*, 1220-1228.

[44] Kreitler, D. F., Mortenson, D. E., Forest, K. T., and Gellman, S. H. (2016) Effects of Single alpha-to-beta Residue Replacements on Structure and Stability in a Small Protein: Insights from Quasiracemic Crystallization, *J. Am. Chem. Soc. 138*, 6498-6505.

[45] Reinert, Z. E., Lengyel, G. A., and Horne, W. S. (2013) Protein-like tertiary folding behavior from heterogeneous backbones, *J. Am. Chem. Soc. 135*, 12528-12531.

[46] Horne, W. S., Price, J. L., and Gellman, S. H. (2008) Interplay among side chain sequence, backbone composition, and residue rigidification in polypeptide folding and assembly, *Proc. Natl. Acad. Sci. USA 105*, 9151-9156.

[47] Lengyel, G. A., and Horne, W. S. (2012) Design strategies for the sequence-based mimicry of side-chain display in protein beta-sheets by alpha/beta-peptides, *J. Am. Chem. Soc. 134*, 15906-15913.

[48] Arnold, U., Huck, B. R., Gellman, S. H., and Raines, R. T. (2013) Protein prosthesis: beta-peptides as reverse-turn surrogates, *Protein Sci. 22*, 274-279.

[49] Arnold, U., Hinderaker, M. P., Nilsson, B. L., Huck, B. R., Gellman, S. H., and Raines, R. T. (2002) Protein prosthesis: a semisynthetic enzyme with a beta-peptide reverse turn, *J. Am. Chem. Soc. 124*, 8522-8523.

[50] Daura, X., Gademann, K., Schäfer, H., Jaun, B., Seebach, D., and van Gunsteren, W. F. (2001) The β-Peptide Hairpin in Solution: Conformational Study of a β-Hexapeptide in Methanol by NMR Spectroscopy and MD Simulation, *J. Am. Chem. Soc. 123*, 2393-2404.

[51] Mayer, C., Muller, M. M., Gellman, S. H., and Hilvert, D. (2014) Building proficient enzymes with foldamer prostheses, *Angew. Chem. Int. Ed. Engl. 53*, 6978-6981.

[52] Mortenson, D. E., Kreitler, D. F., Thomas, N. C., Guzei, I. A., Gellman, S. H., and Forest, K. T. (2018) Evaluation of beta-Amino Acid Replacements in Protein Loops: Effects on Conformational Stability and Structure, *Chembiochem 19*, 604-612.

[53] Tsien, R. Y. (1998) THE GREEN FLUORESCENT PROTEIN, *Annu. Rev. Biochem. 67*, 509-544.

[54] Schwede, T. F., Rétey, J., and Schulz, G. E. (1999) Crystal Structure of Histidine Ammonia-Lyase Revealing a Novel Polypeptide Modification as the Catalytic Electrophile, *Biochemistry 38*, 5355-5361.

[55] Kumar, S., Prakash, S., Gupta, K., Dongre, A., Balaram, P., and Balaram, H. (2016) Unexpected functional implication of a stable succinimide in the structural stability of *Methanocaldococcus jannaschii* glutaminase, *Nat. Commun. 7*, 12798.

[56] Roth, C., Weizenmann, N., Bexten, N., Saenger, W., Zimmermann, W., Maier, T., and Strater, N. (2017) Amylose recognition and ring-size determination of amylomaltase, *Sci. Adv. 3*.

[57] Acedo, J. Z., Bothwell, I. R., An, L., Trouth, A., Frazier, C., and van der Donk, W. A. (2019) O-Methyltransferase-Mediated Incorporation of a beta-Amino Acid in Lanthipeptides, *J. Am. Chem. Soc. 141*, 16790-16801.

[58] Janetzko, J., and Walker, S. (2017) Aspartate Glycosylation Triggers Isomerization to Isoaspartate, *J. Am. Chem. Soc. 139*, 3332-3335.

[59] Deverman, B. E., Cook, B. L., Manson, S. R., Niederhoff, R. A., Langer, E. M., Rosova, I., Kulans, L. A., Fu, X. Y., Weinberg, J. S., Heinecke, J. W., Roth, K. A., and Weintraub, S. J. (2002) Bcl-X-L deamidation is a critical switch in the regulation of the response to DNA damage, *Cell 111*, 51-62.

[60] Lee, J. C., Kang, S. U., Jeon, Y., Park, J. W., You, J. S., Ha, S. W., Bae, N., Lubec, G., Kwon, S. H., Lee, J. S., Cho, E. J., and Han, J. W. (2012) Protein L-isoaspartyl methyltransferase regulates p53 activity, *Nat. Commun. 3*.

[61] Curnis, F., Longhi, R., Crippa, L., Cattaneo, A., Dondossola, E., Bachi, A., and Corti, A. (2006) Spontaneous formation of L-isoaspartate and gain of function in fibronectin, *J. Biol. Chem. 281*, 36466-36476.

[62] Mallagaray, A., Creutznacher, R., Dulfer, J., Mayer, P. H. O., Grimm, L. L., Orduna, J. M., Trabjerg, E., Stehle, T., Rand, K. D., Blaum, B. S., Uetrecht, C., and Peters, T. (2019) A post-translational modification of human Norovirus capsid protein attenuates glycan binding, *Nat. Commun. 10*.

[63] Lindner, H., Sarg, B., Grunicke, H., and Helliger, W. (1999) Age-dependent deamidation of H1(0) histones in chromatin of mammalian tissues, *J. Cancer. Res. Clin. Oncol. 125*, 182-186.

[64] David, C. L., Keener, J., and Aswad, D. W. (1999) Isoaspartate in ribosomal protein S11 of *Escherichia coli*, *J. Bacteriol. 181*, 2872-2877.